Biomedical Signal Processing and Control 68 (2021) 102781

Contents lists available at ScienceDirect

Biomedical Signal Processing and Control

journal homepage: www.elsevier.com/locate/bspc

sEMG-based consecutive estimation of human lower limb movement by using multi-branch neural network

Xingjian Wang [a,b,*], Dengpeng Dong [a], Xiaokai Chi [a], Shaoping Wang [a,b], Yinan Miao [a], Mailing An [a], Alexander I. Gavrilov [c]

[a] the School of Automation Science and Electrical Engineering, Beihang University, Beijing 100191, China
[b] Beijing Advanced Innovation Center for Big Data-based Precision Medicine, Beihang University, Beijing 100191, China
[c] Bauman Moscow State Technical University, Department of Automatic Control Systems, Moscow 105005, Russia

ARTICLE INFO

Keywords:
Surface EMG
Gait phases recognition
Joint angle estimation
Multi-branch neural network

ABSTRACT

Surface electromyography (sEMG) has the potential for human lower limb movement analysis, including gait phases recognition and joint angle estimation, which can provide a great level of human interaction with the exoskeleton orthotic devices. In this paper, a method based on deep learning is proposed, which maps the multichannel sEMG signals to human lower limb movement, including 4 different gait phases and 3 flexion/extension joint angles. First, five time-domain features and spectrogram data as frequency domain features are extracted from the sEMG data from 8 muscles of right legs. Then, a multi-branch neural network (MBNN) with convolutional neural layers and recurrent neural layers is constructed, which uses both the extracted features and raw data as input to analyze human movement. Experimental results show that the mean accuracy of classification of our proposed methods can reach high level ($90.92 \pm 3.58\%$ for speed dependent and $85.04 \pm 5.14\%$ for speed independent). Meanwhile, average of the root mean square error between estimated and real joint angles is (3.75 ± 1.52 degree for speed dependent and 6.12 ± 2.54 degree for speed independent). These results indicate that the proposed method can be used to facilitate adoption of exoskeleton orthotic device in real-life applications, with gait phases determining impedance characteristic of devices and angles estimating joint movement.

1. Introduction

As the development of technology, robotic devices like exoskeleton orthotic device for rehabilitation in addition to traditional therapies is getting more and more attention. One of the largest challenges needed to be overcome in such devices is the user interface and control [1]. Therefore, satisfactory degree in the sense of comfort and movement symmetry during walking has become an increasing interest in the research field. Correct movement analysis can be considered as the basic of synchronous control of exoskeleton orthotic devices. In addition, movement analysis plays a significant role in several scientific research and application, such as classification of daily life activities [2], sports medicine [3] and evaluation of gait status to distinguish between normal and pathological gait [4,5].

Walking process of a person is characterized by periodicity, repeatability and continuity, thus the consecutive estimation joint angles can achieve smooth control of exoskeleton robot. Besides, the joint impedance is various in different gait phases, which means gait phases recognition is an important factor in lower limb exoskeleton control. Rancho Los Amigos gait analysis committee [6] proposed a frequently used terminology, which divided phase of walking motion into initial contact (IC), loading response (LR), mid stance (MSt), terminal stance (TSt), pre swing (PSw), initial swing (ISw), mid swing (MSw) and terminal swing (TSw). The first five phase comprise the stance phase (ST) and the last three comprise the swing phase (SW). Thus, due to the complex and dynamic characteristics of walking process, the improvement of lower limb movement analysis remains an issue to be addressed.

Recently, there are various studies focusing on lower limb movement analysis during walking with methods generally based on wearable or non-wearable sensors [7–9].

For the non-wearable sensors, researchers mainly focused on studies of vision based systems [10–12], force platform [13–15] and ultrasonic sensor [16,17]. Although non-wearable sensors remain the most accurate system to perform gait analysis [18], they have limitation of using outdoor environment [19]. Therefore, wearable sensors are more largely used for application at present.

* Corresponding author at: the School of Automation Science and Electrical Engineering, Beihang University, Beijing 100191, China.
E-mail address: wangxj@buaa.edu.cn (X. Wang).

https://doi.org/10.1016/j.bspc.2021.102781
Received 20 July 2020; Received in revised form 28 April 2021; Accepted 15 May 2021
Available online 31 May 2021

For the wearable ones, movement analysis methods widely imposed are based on ground reaction force (GRF) sensors, inertial measurements unit (IMU) and sEMG sensors. GRF sensors based on footswitch or foot pressure insole represents the brief method in gait recognition, whose output directly shows the gait phase [20,21]. However, GRF-based methods have difficulties to estimate joint angles because it's difficult to model human lower extremity. IMU-based methods are more popular in recent years for its high performance. IMU is combination of accelerometers and gyroscopes, which can compensate for the data drift error comparing to usage with only one of them [22–24]. But IMU is difficult to predict joint angles, because kinetics data has the hysteretic nature.

Comparing to mechanical parameters, biological signals like sEMG have the advantage to be accessible before muscle producing movement. Therefore, using biological signal is more possible to predict lower limb movement for their direct relation to user intention [25,26]. As a result, sEMG signals are considered to be a valuable method in recognizing lower limb movements [27–30]. For gait phases recognition, Courtine et al. [31] evaluate the sEMG features of different muscles between stance and swing phases during straight walking and turning. Lauer et al. [32] designed a fuzzy interface system and a supervisory control system to predict five gait events of the child with cerebral palsy, which demonstrated the ability of the controller to predict gait events to within 82 ms on average. Lee et al. [33] established a gait phase recognition system that is capable of rigidly controlling ill effects by carrying out a large-scale analysis that combined statistical, model-based and empirical approaches, which formulated a guideline for design of highly reliable sEMG signal-based walking assistant systems in a variety of smart home scenarios. For joint angles estimation, Zhang et al. [28] built a simple BP neural network to describe the relationship between sEMG signals and joint angles of human lower limb with the RMSE for treadmill exercise less than 6 degree. Chen et al. [34] constructed regression model to relate the multichannel sEMG signals to human lower limb joint angles and reduced by 50% of the root mean square error between the estimated joint and calculated ones.

Although sEMG signal based method is an effective solution to operate exoskeletons, this kind of data is not as popular as other wearable sensor systems due to its non-stationary and sensitivity [35,36]. In addition, the feature extraction procedure has been given widespread attention all the time.

In recent years, deep learning algorithms have demonstrated impressive power in various research fields, which has the ability to extract significant features on multiple levels of representation and complete complex tasks. In this paper, a method based on deep learning algorithm with feature extraction and feature learning is proposed to analyze human lower limb movement while walking. The movement analysis contains gait phases recognition and joint angles estimation, which can determine impedance characteristic and joint angles for exoskeleton control. The remainder of this paper is organized as follows. In Section 2 we first introduce the experiment protocol and sEMG equipment for data acquisition and various artificial feature extraction approaches are presented. Then we describe our method-MBNN-in detail. After that, the deep learning algorithm based on MBNN is used for two movement analysis strategies. In Section 3 we validate our results and outline the analyses from different aspect. In Section 4 we discuss our experimental results. Finally, conclusions are presented in Section 5.

2. Experiments and methods

2.1. Data acquisition

This study was approved by the corresponding Institutional Review Boards, and all participants signed an informed consent form prior to participating. Three able-bodied persons were selected in this study, with height ranging from 170 to 175 cm and weight ranging from 65 to 80 kg. The participants were required to walk on a treadmill with speeds of 3, 3.5, 4 km/h. Each trial was repeated 2 times and each time required 6 min. During each trial, the signals were collected with a wireless instrument (Noraxon Desktop DTS-8) at the sample rate of 1500 Hz. According to the recommendations of SENIAM [37] and the method from [38], Eight sEMG Ag/AgCl electrodes were placed on the surfaces of eight right lower limb muscles, which were precleaned using alcohol. The diameter of the electrode was 10mm. And the muscles selected were rectus femoris (RF), vastus lateralis oblique (VLO), vastus medialis oblique (VMO), biceps femoris (BF), semitendinosus (ST), tibialis anterior (TIA), lateral gastrocnemius (LGA) and medial gastrocnemius (MGA). And four footswitches were taped to either side of sole to collect gait phase signals, which also collected by Noraxon Desktop DTS-8. The sensor placement is shown in Fig. 1 (a) and (b). The signals were sent to a desk receiver in real-time and stored as raw data. Meanwhile, joint angle information is collected with an 8-camera opto-electronic system (VICON). The sample rate is 150Hz and marker positions are introduced in Fig. 1 (c) and Table 1. To reduce the size of dataset, we only choose 10% of data from each trial. The above two systems have corresponding software at the PC end, which is MR3 and Nexus. The two sets of system signals can be synchronously collected, recorded, and analyzed on Nexus software to ensure the synchronization of the signal and reduce the signal error caused by software and hardware.

The correspondence between source (sEMG signals) and subject movement (gait phases and joint angles) is shown in Fig. 2. For four gait phases recognition, when in the IC stage, the main muscle generating power is RF, VLO, VMO, BF, ST and MGA. In MSt stage, both TIA and LGA produce higher frequency signals while signal of VMO has a low frequency wave. From the curve, we can find a few characters in TSt stage - only a high frequency fluctuation generates in TIA and LGA in early time. In the SW stage, ST is more active than other stage because the muscle support power to bend the knee. The range of angle of hip joint is -15° to 30°, while knee joint is -12° to 45° and ankle joint is -20° to 8°, whose ranges almost agree with [39].

2.2. Data processing

The frequency power of sEMG signals is located between 0 and 500 Hz, hence the raw sEMG data were band-pass filtered using a second order Butterworth filter with a frequency ranging between 0 and 500 Hz. In addition, a 50Hz notch filter was used to eliminate the power content noise. In addition to using filtered data, we extract time-domain features and frequency-domain features as input to our model. Time-domain features like root-mean-square, auto regression model, and waveform length have improved the sEMG classification accuracy involving lower limb movements compared to typical frequency-domain feature [40]. However, the frequency-domain methods such as short time Fourier transform, wavelets transform and Hilbert-Huang transform are widely used in movement pattern recognition based on sEMG and achieve a result of high accuracy. Time-domain features contain the brief and concentrated information of the signal, while frequency-domain can describe the relationship between frequency structure and the amplitude of the signal. To meet the real-time recognition requirement, the length of sliding window is 250 sample points. The sliding step is 15 sample points, which means that a new sEMG data segment is generated every 15 sample points (10 ms). Particularly, the following set of features was derived from an sEMG data segment.

2.2.1. Time-domain features

We extract five time domain features of each channel, including waveform length (WL), mean absolute value (MAV),Variance (VAR), root mean square (RMS) and zero crossing (ZC). The waveform length is defined as cumulative change of amplitude in each segment, which is calculated as

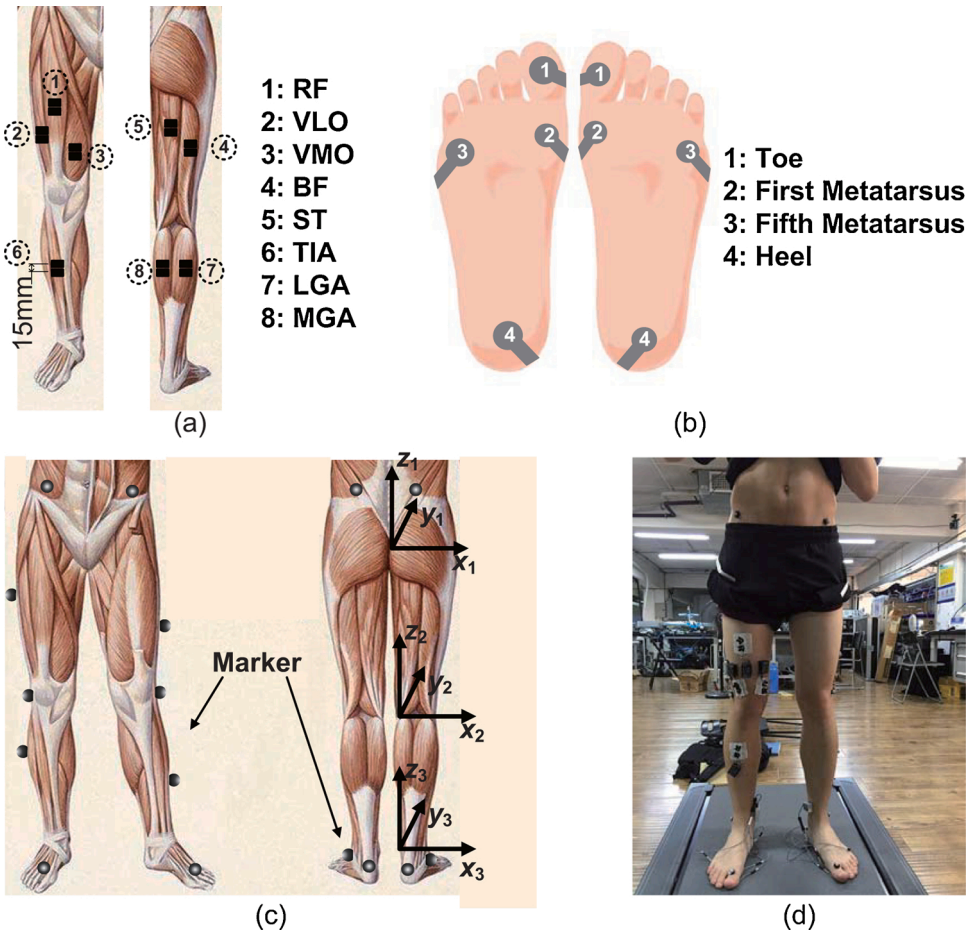

Fig. 1. Placement of the sensor: (a) sEMG electrodes attached on right leg. (b) Pressure sensors taped to either side of sole. (c) The motion capture marker placement. (d) Experimental setup with a subject walking on a treadmill.

Table 1
Position numbers and the corresponding names of marker positions for motion capture.

No.	Position	No.	Position
1	Left anterior superior iliac spines	9	Left heel
2	Left posterior superior iliac spines	10	Left toe
3	Right anterior superior iliac spines	11	Right thigh
4	Right posterior superior iliac spines	12	Right knee
5	Left thigh	13	Right tibia
6	Left knee	14	Right ankle
7	Left tibia	15	Right heel
8	Left ankle	16	Right toe

$$\mathrm{WL} = \sum_{k=1}^{N-1} |x_{k+1} - x_k|$$

Finally, the features constitute a time-domain matrix of 5×8, which is

$$F = \begin{bmatrix} \mathrm{WL_{RF}} & \cdots & \mathrm{WL_{MGA}} \\ \vdots & \ddots & \vdots \\ \mathrm{ZC_{RF}} & \cdots & \mathrm{ZC_{MGA}} \end{bmatrix}$$

2.2.2. *Frequency-domain feature*

The spectrogram for each segment is used as the frequency-domain feature as the part of input to the classifier. Using a 64-point short time Fourier transform (STFT) with a Hann window and 32-point overlap. Zero filling operation is performed for each segment. Therefore, each segment of the spectrogram is calculated at a 33 different frequencies (0–750 Hz) with 9 time bins. Thus, the spectrogram of each segment resulted in a matrix of 33 × 9 × 8 (frequency × time × channels). We kept only the first 9 rows of the frequency spectrogram (0–187.5 Hz) because the majority of signal energy mainly distributes within frequency range from 0 to 200 Hz. As a result, each spectrogram matrix has a dimension of 9 × 9 × 8.

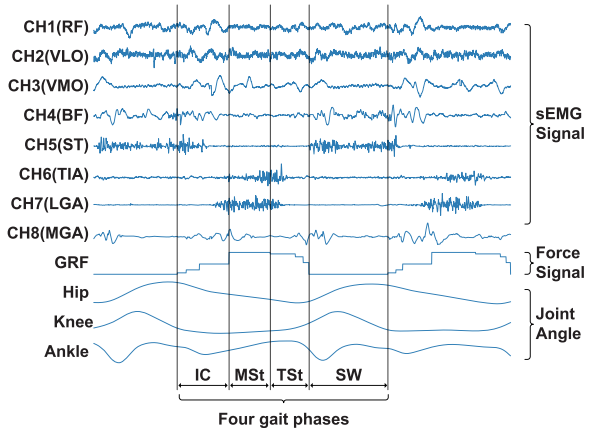

Fig. 2. The relationship between sEMG signals and movement of one subject.

2.3. *Multi-branch neural network*

The multi-branch neural network (MBNN) model with multi-feature as input is proposed to estimate both human gait phases and joint angles

continuously. In this method, sEMG signals are collected with the surface electrodes from eight right lower limb muscles. First the signals are preprocessed as raw data. Then a set of time-domain features and a frequency-domain feature of the data are calculated, which can provide some specific information. Meanwhile, we utilize neural network for feature learning to obtain information autonomously. With convolutional neural network (CNN), recurrent neural network (RNN) and combination of them (RCNN), the MBNN is employed to process different kinds of information to map the sEMG signals into human movement, including four gait phase (SW, IC, MSt and TSt) and three kinds of joint angles (hip angle, knee angle and ankle angle). The overall schematic of the method is shown in Fig. 3. With time-domain features as input, network RNN contains 3 recurrent layers using gated recurrent unit (GRU) [41], which can adaptively capture dependencies of different time scales. Using the update gate and reset gate, the GRUs have the ability to selectively pass information of the sEMG signal across time steps with hidden states. The activation $\mathbf{h}_t$ of GRU at time t is a linear interpolation between the previous activation $\mathbf{h}_{t-1}$ and the candidate activation $\widetilde{\mathrm{h}}_t$.

$$\mathrm{h}_t = \mathrm{z}_t \odot \mathrm{h}_{t-1} + (1 - \mathrm{z}_t) \odot \widetilde{\mathrm{h}}_t \tag{1}$$

where $\odot$ is an element-wise multiplication where the update gate $\mathbf{z}_t$ determines the number of the units to update its activation. Thus, the update gate can be used to control the amount of information from previous state transferred to current state. The update gate is calculated as

$$\mathrm{z}_t = \sigma(\mathrm{W}_z \mathrm{x} + \mathrm{U}_z \mathrm{h}_{t-1}) \tag{2}$$

where $\mathbf{h}_{t-1}$ is the hidden state from previous time t-1.

$\mathbf{r}_t$ is a set of reset gates, which determines how much information from previous state is written to the candidate activation. Similarly, it can be computed by

$$\mathrm{r}_t = \sigma(\mathrm{W}_r \mathrm{x} + \mathrm{U}_r \mathrm{h}_{t-1}) \tag{3}$$

The candidate activation determines how much past information to be stored, which is shown as follows

$$\widetilde{\mathrm{h}}_t = tanh(\mathrm{W}_h \mathrm{x} + \mathrm{r}_t \odot \mathrm{U}_h \mathrm{h}_{t-1}) \tag{4}$$

The number of the hidden cells of the first and second layer are 32 and 64 respectively and all of the hidden states are used as the inputs of the next layer. For the third layer, the number of the hidden cells is 128 and only the last hidden state is passed, which will be merged later.

The input of second network, spectrogram, is processed by using two dimensional (2D) CNN. In this way, each of the spectrogram is treated like an image and the 8 channels mimic the color channels of the image. 2D CNN has been applied to sEMG data for classification of movements of hands [36,42,43] to accelerate the training procedure and the result showed the high performance of this method. 2D CNN used in this paper is composed of the following parts. First, it includes two convolutional layers with 16 as well as 32 filters of size 3×3 respectively, and either of them connects a subsampling layer that performs a maximum pooling with filters of 2×2. Second, it includes a flattening layer used to flatten data in order to enable it to be merged later. Because of the high dimension and complexity of the frequency-domain feature, this part of network does not contain recurrent layers to pass historical information.

In order to extract still more valuable information from the sEMG signals, the filtered data is used as input to a third neural network structure (RCNN). RCNN contains 2 convolutional layers, 2 maximum pooling layers and 3 recurrent layers. The 1D convolutional layers can extract features from regional input and recognize local patterns from the sEMG sequence. A pattern learned at a former position can later be recognized at a different position because of the same input transformation performed on every sequence, making 1D CNN translation invariant for temporal translations. The 1D discrete convolution can be defined as

$$y_k = h(k) * u(k) = \sum_{i=1}^{N} h(k-i)u(i) \tag{5}$$

Therefore, the output of the convolutional unit can be calculated as

$$y_{i,k} = \sigma\left(\sum_{n=1}^{N}\sum_{j=i}^{i+2} \omega_{j,n} u_{j,n} + b_{i,k}\right), k = 1, 2, \ldots K \tag{6}$$

The following layers of the convolutional layer is the max-pooling layer, whose unit can be computed as

$$p_{h,k} = \max_{l=h,\ldots,h+S-1}(y_{l,k}) \tag{7}$$

where S is the pooling size, and S=3 in this method.

The convolution neural network proposed in this paper has four layers. It includes two convolutional layers with 16 as well as 32 filters of size 3 respectively, and either of them connects a subsampling layer that performs a maximum pooling with filters of 3.

The features extracted from the 1D convolutional layers are used as the input of the recurrent layers of the same structure of part RNN, except the hidden units. The number of hidden units of three recurrent layers in RCNN are 32, 64 and 128 respectively.

The output of three network above is concatenated to a vector and delivered to the fully connected layer 1, directly connected by the output layer for three joint angles. Meanwhile, a dropout layer and a fully connected layer with soft-max units as activation function are applied after the fully connected layer 1 to classify the sEMG signal to gait patterns.

As result, the detail structure of the classification system is shown in Fig. 4.

2.4. Movement analysis

Speed-dependent and speed-independent cases were tested and compared. For speed-dependent, it was tested from the dataset of each subject at each speed individually. The proposed MBNN model was trained on 80% data from each subject with each trial introduced above, and tested on the 20% of the leave-out data. In order to analyze robustness of the method, data of one trial was divided into 5 parts, where 4 parts were selected as the training set and the other part was set as the testing set. This was repeated 5 times so that each data set was

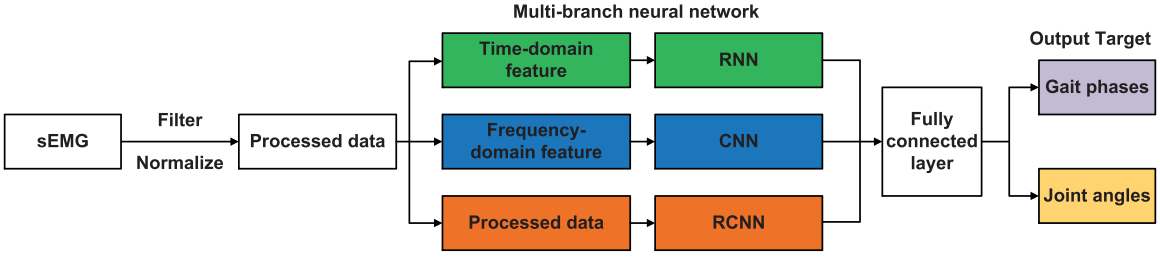

Fig. 3. Schematic representation of the movement analysis system.

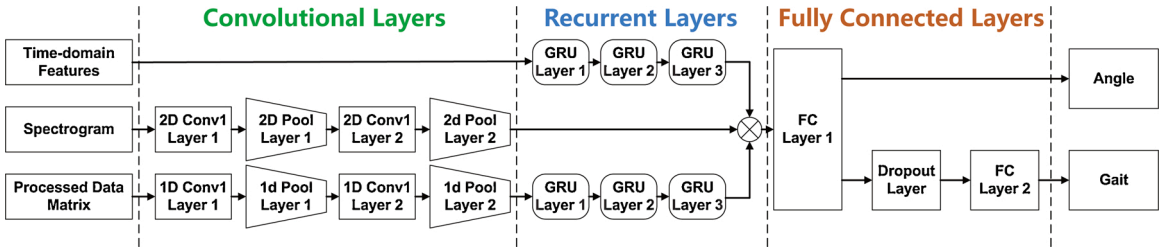

Fig. 4. Structure of classifier with deep neural network.

tested once. For speed-independent, it was tested from the dataset of one subject which is the combination of all speeds. The dataset was divided into 10 parts, where 9 parts were selected as the training set and the other part was set as the testing set. This was repeated 10 times and all the three subjects were estimated.

2.5. Performance evaluation

A confusion matrix is provided here for the visualization of the classification system performance. With each row of the matrix **M** denotes the percentage of instances in a real class and each column implies the percentage of a predicted class, the matrix **M** is defined as

$$\mathrm{M} = \begin{bmatrix} C_{00} & C_{01} & C_{02} & C_{03} \\ C_{10} & C_{11} & C_{12} & C_{13} \\ C_{20} & C_{21} & C_{22} & C_{23} \\ C_{30} & C_{31} & C_{32} & C_{33} \end{bmatrix} \tag{8}$$

As the correct predictions are located on the diagonal of the confusion matrix, the false predictions can be analyzed visually from the other elements. For example, an element of the matrix can be computed as follows:

$$C_{01} = \frac{N_{01}}{N_0} \times 100\% \tag{9}$$

where N_{01} denotes the amount of state 0 predicted as state 1 and N_0 is the total cases predicted as state 0.

In addition, for the multi-labeled task, macro-average and micro-average are usually used to measure the performance of the classifier [44]. Here the macro-average precision (MAP), macro-average sensitivity (MAS), macro-average F1 (MAF1), micro-average precision (MIP), micro-average sensitivity (MIS) and micro-average F1 (MIF1). Respectively the indicators are defined by

$$P_{\mathrm{MAP}} = \frac{1}{n}\sum_{i=1}^{n} P_i \tag{10}$$

$$P_{\mathrm{MAS}} = \frac{1}{n}\sum_{i=1}^{n} S_i \tag{11}$$

$$P_{\mathrm{MAF1}} = \frac{2 \times P_{\mathrm{MAP}} \times P_{\mathrm{MAS}}}{P_{\mathrm{MAP}} + P_{\mathrm{MAS}}} \tag{12}$$

$$P_{\mathrm{MIP}} = \frac{\sum_{i=1}^{n} N_{\mathrm{TP}}^i}{\sum_{i=1}^{n} N_{\mathrm{TP}}^i + \sum_{i=1}^{n} N_{\mathrm{FP}}^i} \times 100\% \tag{13}$$

$$P_{\mathrm{MIS}} = \frac{\sum_{i=1}^{n} N_{\mathrm{TP}}^i}{\sum_{i=1}^{n} N_{\mathrm{TP}}^i + \sum_{i=1}^{n} N_{\mathrm{FN}}^i} \times 100\% \tag{14}$$

$$P_{\mathrm{MIF1}} = \frac{2 \times P_{\mathrm{MIP}} \times P_{\mathrm{MIS}}}{P_{\mathrm{MIP}} + P_{\mathrm{MIS}}} \tag{15}$$

where

$$P_i = \frac{N_{\mathrm{TP}}^i}{N_{\mathrm{TP}}^i + N_{\mathrm{FP}}^i} \times 100\%,$$

$$S_i = \frac{N_{\mathrm{TP}}^i}{N_{\mathrm{TP}}^i + N_{\mathrm{FN}}^i} \times 100\%$$

and i=1,2,…, n denotes the classes of the gait events. N_{TP}, N_{FP}, N_{FN} denotes number of true positive, false positive and false negative outcome of the classifier respectively.

In order to describe the estimation precision quantitatively, RMSE η, the cross-correlation coefficient (CCC) ρ and R-Square $R2$ between estimated and calculated joint angle values are used and can be calculated as (the formulas are suitable for any joint)

$$\eta = \sqrt{\frac{\sum_{i=1}^{N}(\widetilde{\theta}_i - \theta_i)^2}{N}} \tag{16}$$

$$\rho = \frac{\sum_{i=1}^{N}(\theta'_i - \overline{\theta}')(\theta_i - \overline{\theta})}{\sqrt{\sum_{i=1}^{N}(\theta'_i - \overline{\theta}')^2}\sqrt{\sum_{i=1}^{N}(\theta_i - \overline{\theta})^2}} \tag{17}$$

$$R2 = 1 - \frac{\sum_{i=1}^{N}(\widetilde{\theta}_i - \theta_i)^2}{\sum_{i=1}^{N}(\theta_i - \overline{\theta})^2} \tag{18}$$

where $\overline{\theta}'$ is the mean value of the estimated joint angles, and $\overline{\theta}$ is the mean value of the target joint angles, and N represents the number of samples used in the computation.

3. Results

3.1. Evaluation of the MBNN structure

In order to evaluate the structure of the classification system, a series of dataset was trained and tested in the experiments. While it is difficult to analyze the best structure of the neural network, the results shown following provide the good performance of the method proposed in this paper and guidance to design a much better network. First, the effect of different features as input of the MBNN is considered in this paper. For gait phases recognition, Fig. 5 (a) shows the comparison of the accuracy of classifier with MBNN (all features, AF), RCNN (raw data, RD), RNN (time-domain features, TF) and CNN (frequency-domain feature, FF). The model based on RD as input equal to a RCNN model. For the model simply with TF, it becomes a multi-layer RNN and for the model only with FF, it becomes a traditional CNN. The model with AF as input ranks high of average accuracy, which are $92.39 \pm 2.17\%$ for four gait phases recognition. The accuracy ranks between 88.4% to 96.8% of all the experiments in speed-dependent cases using this type of method. System with TF has the least accuracy, the reason may be that the current RNN network with the number of GRU unit cannot learn effective information from the complex sEMG signal. For evaluation of joint angles, Fig. 5(b) shows the comparison of the RMSE for different networks. MBNN also achieves the best result of the lowest RMSE, which is 3.48 ± 1.36 degree for three joints. As a result, combining with different features could improve performance and robustness of the classifier.

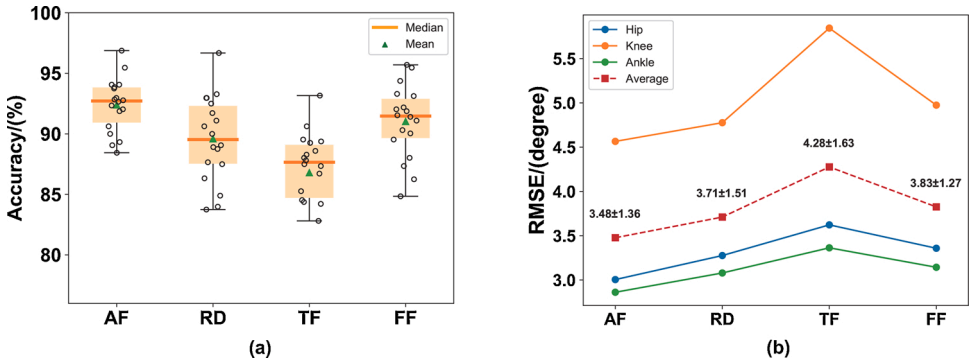

Fig. 5. Effects of different features as input for the neural network.

3.2. Performance of the MBNN model

3.2.1. Speed-dependent estimation

Comparisons between continuous prediction and real lower limb movement are shown in Figs. 6 and 7 respectively. It's noted that we chose one of the data sets as an example here. The gait phases prediction of the MBNN model was almost matched the reality, while incorrect results mainly distributed in regions where transition between different phases. For joint angles estimation, the prediction and real curves show very close variation trends. The prediction of the joint angles has more fluctuation in maximum and minimum of the curve. However, this type of fluctuation can be improved later for the control of exoskeleton.

The overall average and standard of the four gait phases recognition are shown in Table 2. The dataset collected from each subject in each trial is split into 80% of training data and 20% of testing data. All the data of three subjects were performed with a five fold cross validation respectively.The test data achieve the average accuracy of $90.92 \pm 3.58\%$. Consistent with the result shown in Fig. 6, average of SW and TSt phases are much higher than IC and MSt phases. The accuracy of SW and TSt phases reach $95.23\% \pm 5.45\%$ and $92.27\% \pm 5.19\%$ respectively, while IC and MSt phases reach $85.45\% \pm 11.84\%$ and $83.31\% \pm 13.05\%$ respectively. The wrong predicted IC phase is mainly SW and MSt phases in real and the wrong predicted MSt phase is mainly IC phase. From our perspective, the reason is that IC and MSt phases have some similarity in the features of the sEMG signals.

The macro-average and micro-average metrics are shown in Table 3. Macro-average F1 and micro-average F1 are about 90%, which mean that the classifier has good classification performance. But macro-average is a litter lower than micro-average, which indicate the state of small-size samples in one cycle, IC phase, need to be taken care later.

Statistical analysis of joint angles estimation was implemented and the results are shown in Table 4. The RMSE η is about 3.26, 4.95 and 3.04 degree for FE hip, knee and ankle angles respectively. The low RMSE, high CCC and high R2 show the good performance of the MBNN model. The CCC and R2 of ankle joint is the lowest which imply that the performance of the system for ankle joint angle is worse than others, with the reason that curve of ankle angle is much more complicated.

Compared with the result of holdout validation in Fig. 5, the prediction result of five fold cross validation is almost the same, which is about 1.47% lower than holdout validation of gait phase recognition and 0.27 degree higher than holdout validation of average joint angles. This shows that the MBNN model has good robustness

3.2.2. Speed-independent estimation

Data with different walking speed of one subject was combined and divided into two datasets, including 90% of training data and 10% of testing data. All the data of three subjects were performed with a ten fold cross validation respectively. The results are presented in Tables 5–7. Compared with the speed-independent cases, the average accuracy of gait recognition decreases by about 5.9%, which is 85.04%. From Table 5, we could find that test accuracy of SW and TSt phases could reach 93.83% and 85.91% respectively. However, accuracy of IC and MSt phases declined considerably. Macro-average and micro-average shown in Table 6 indicate that macro-average is lower than micro-average, which means states of small-size samples have influence in both precision and sensitivity.

The RMSE, CCC and R2 shown in Table 7 indicates the performance goes down a little in speed-independent cases, because joint angles vary in different walking speed. The CCC and R2 of hip and knee angles shows that the predicted angles could almost match the real angles. However, for the ankle angles with much more complicated trend, the CCC and R2 drop significantly.

4. Discussion

This study presents an approach based on MBNN to use lower limb

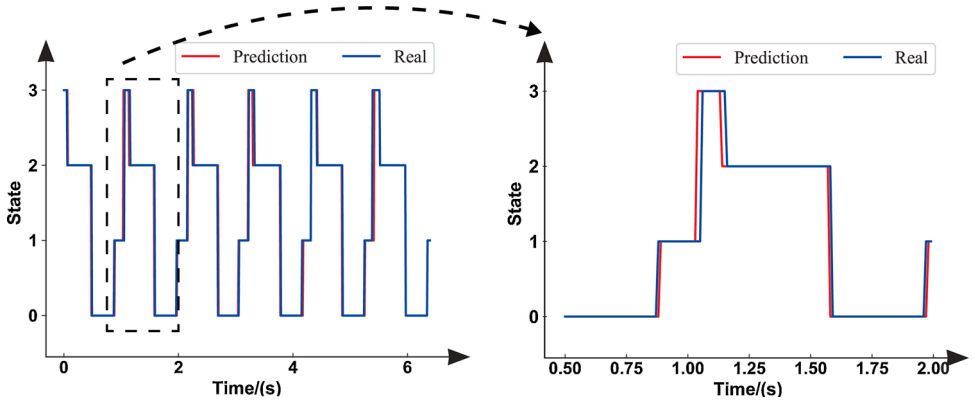

Fig. 6. The gait recognition of one subject in one walking trial.

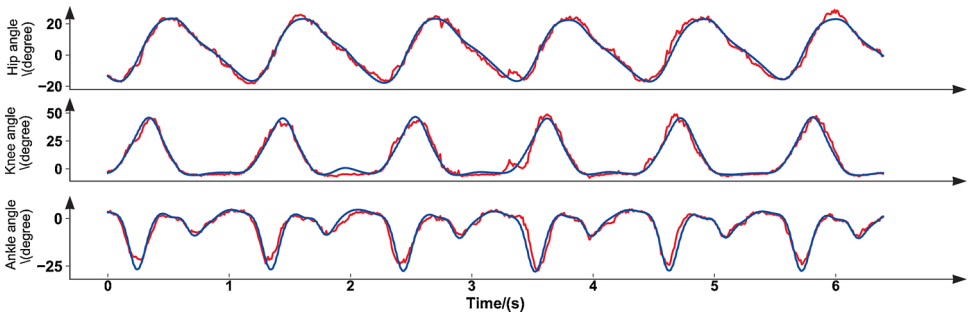

Fig. 7. The estimated joint angles of one subject in one walking trial.

Table 2
Overall mean and STD of classifier performance metrics in percentage for four gait phases recognition in speed-dependent case.

Class		Predicted			
		SW(S0)	IC(S1)	TSt(S2)	MSt(S3)
Real	SW	95.23 ± 5.45	4.06 ± 5.16	2.01 ± 1.84	0.02 ± 0.15
	IC	2.58 ± 2.51	85.45 ± 11.84	0.36 ± 1.36	10.82 ± 10.60
	TSt	2.14 ± 5.07	3.14 ± 0.18	92.27 ± 5.19	5.85 ± 5.76
	MSt	0.04 ± 0.21	10.04 ± 10.50	5.35 ± 4.59	83.31 ± 13.05

Table 3
Mean multi-labeled performance task metrics in percentage for four gait phases recognition in speed-dependent case.

MAP		MIP		MAS		MIS		MAF1		MIF1	
μ	σ	μ	σ	μ	σ	μ	σ	μ	σ	μ	σ
89.07	4.06	91.92	3.61	88.64	4.26	91.92	3.61	88.84	4.00	91.92	3.61

Table 4
Root mean square error η, cross-correlation coefficient ρ and R-Square $R2$ of joint angles estimation in speed-dependent case.

θ	η/degree		ρ		R2	
	μ	σ	μ	σ	μ	σ
θ_{hip}	3.26	1.33	0.97	0.03	0.93	0.07
θ_{knee}	4.95	1.59	0.96	0.03	0.91	0.07
θ_{ankle}	3.04	0.74	0.91	0.04	0.84	0.08

sEMG signals to consecutively predict gait phases and estimate joint angles during walking. The network structure proposed in this paper contains three different parts. Combining 1D CNN and RNN as RCNN, we utilize method based on feature learning to extract features from sEMG signals to decrease information loss. Meanwhile, time-domain and frequency-domain features are used as input of the MBNN to add definitive information, which can improve robustness for the classifier. The results in our experiment show that with three different features, the classifier has good performance with an average of 90.92 ± 3.58% for speed dependent and 85.04 ± 5.14 % for speed independent in four gait phases classification. For joint angles estimation, the RMSE is low, the CCC is high and R2 is close to 1, which means that the model prediction well accords with the real angles. The results support that the network framework could be a useful tool to classify gait movement with sEMG signals.

Compared with other linear and nonlinear algorithm, deep learning method has good performance in image processing, speech recognition and so on. In this paper, combining CNN and RNN, the system establishes a complex function for the map between sEMG signals and lower limb movement. CNN has the ability to transform lower-level features to high-level ones as well as improve the speed of classifying time, which is efficient in extracting features from the sEMG data and spectrum. Since lower limb movement are sequences changing over time, RNN can selectively pass and contain information over time steps. For movement analysis based on sEMG signals, there are some research using CNN or RNN structure to complete tasks and offer a better performance [36,45]. However, most of the study focused on hand movement because lower limb movement classification based on sEMG signals has more difficulty. Signals of lower limb are more complex inherently, because the muscles involved are buried deeply under the skin and overlap with each other [38,46,47]. In this study, we proposed a neural network model with different neural unit to achieve this challenging task, and the system presents a good performance. Compared to the method in [48], the method proposed in this paper can offer an average of 11.9% increase in accuracy of four gait phases recognition. For joint angle estimation, our method has a higher RMSE compared to the method in [34]. However, they need to collect EMG signals in 10 channels, which is two more than we do and they can only predict joint angles during walking cycles.

For this study, gait phases with small samples in the training sets have a poorer performance than the other ones, especially for IC phases recognition. From our perspective, there are two main factors for this negative result. The first one is the complex change of the sEMG signals during gait cycles. For example, sEMG signals of IC stage and the start of MSt stage are nearly the same sometimes, which means the features extracted from data could hardly be classified. The second significant factor is the short-time gait phases have fewer samples in data set. Due to the unbalanced amount of samples in the training set, the generalization of the model on the test set may be not good. The performance of this kind of task could be improved in future studies with some effective method, such as increasing the weights of the class with small samples and decreasing the large ones.

5. Conclusion

A MBNN-based analysis system using sEMG data for lower limb movement during walking is introduced in this paper. After processed by

Table 5
Overall mean and STD of classifier performance metrics in percentage for four gait phases recognition in speed-independent case.

Class		Predicted			
		SW(S0)	IC(S1)	TSt(S2)	MSt(S3)
Real	SW(S0)	93.83 ± 4.71	10.73 ± 10.58	4.89 ± 5.19	0.40 ± 1.10
	IC(S1)	3.81 ± 3.54	78.13 ± 15.04	0.87 ± 2.09	13.37 ± 12.93
	TSt(S2)	2.24 ± 3.83	0.36 ± 1.03	85.91 ± 13.18	13.74 ± 19.19
	MSt(S3)	0.11 ± 0.29	10.77 ± 10.27	8.34 ± 9.25	72.48 ± 22.19

Table 6
Mean multi-labeled performance task metrics in percentage for four gait phases recognition in speed-independent case.

MAP		MIP		MAS		MIS		MAF1		MIF1	
μ	σ	μ	σ	μ	σ	μ	σ	μ	σ	μ	σ
82.59	7.29	85.05	5.23	83.23	6.71	85.05	5.23	82.89	6.90	85.25	5.23

Table 7
Root mean square error η, cross-correlation coefficient ρ and R-Square $R2$ of joint angles estimation in speed-independent case.

θ	η/degree		ρ		R2	
	μ	σ	μ	σ	μ	σ
θ_{hip}	5.61	2.11	0.91	0.08	0.81	0.15
θ_{knee}	7.88	2.74	0.88	0.08	0.77	0.19
θ_{ankle}	4.87	1.58	0.76	0.19	0.58	0.26

filtering and normalizing, a set of time-domain features and the spectrogram are extracted from the source data. Finally, the sEMG data is assigned to predict lower limb movement–gait phases and joint angles–with the aid of the MBNN algorithm supplied with different feature sets. On the newly collected dataset, the model using MBNN to process different features achieve a high average accuracy of gait phases classification over 3 participants and low RMSE of joint angles estimation. The results show that the model can be utilized for information perception of human-robot interaction for exoskeleton, with gait phases determining impedance characteristic of devices and angles estimating joint movement.

Future work will focus on improving robustness of the model to be efficiently applied for user-independent lower limb movement analysis. This will provide more challenges due to the greater muscle variability across subjects. In addition, acceleration for the training and analysis session will be conducted for the system to facilitate the use of devices effectively.

Credit author statement

Xingjian Wang: Methodology, Validation, Software, Writing – review & editing.

Dengpeng Dong: Data curation, Validation, Writing – original draft.

Xiaokai Chi: Experiment, Investigation, Writing – original draft.

Shaoping Wang: Supervision, Methodology, Project administration, Funding acquisition.

Yinan Miao: Supervision, Software, Writing – review & editing.

Mailing An: Visualization, Writing – review & editing.

Alexander I. Gavrilov: Supervision, Methodology, Investigation.

Acknowledgments

This work was supported by the National Basic Research Program of China (Grant No. JCKY2018601C107) and the National Natural Science Foundation of China (Grants No. 51675019, 51620105010).

Declaration of Competing Interest

The authors declare that they have no known competing financial interests or personal relationships that could have appeared to influence the work reported in this paper.

References

[1] A.J. Young, D.P. Ferris, State of the art and future directions for lower limb robotic exoskeletons, IEEE Trans. Neural Syst. Rehabil. Eng. 25 (2) (2016) 171–182.
[2] A. Mannini, A.M. Sabatini, Gait phase detection and discrimination between walking-jogging activities using hidden Markov models applied to foot motion data from a gyroscope, Gait Posture 36 (4) (2012) 657–661.
[3] S. Ounpuu, The biomechanics of walking and running, Clin. Sports Med. 13 (4) (1994) 843–863.
[4] N. Abaid, P. Cappa, E. Palermo, M. Petrarca, M. Porfiri, Gait detection in children with and without hemiplegia using single-axis wearable gyroscopes, PLOS ONE 8 (9) (2013) e73152.
[5] B. Mariani, H. Rouhani, X. Crevoisier, K. Aminian, Quantitative estimation of foot-flat and stance phase of gait using foot-worn inertial sensors, Gait Posture 37 (2) (2013) 229–234.
[6] J. Perry, J.R. Davids, Gait analysis: normal and pathological function, J. Pediatr. Orthop. 12 (6) (1992) 815.
[7] R.T. Lauer, B.T. Smith, R.R. Betz, Application of a neuro-fuzzy network for gait event detection using electromyography in the child with cerebral palsy, IEEE Trans. Biomed. Eng. 52 (9) (2005) 1532–1540.
[8] U. Martinez-Hernandez, A.A. Dehghani-Sanij, Adaptive Bayesian inference system for recognition of walking activities and prediction of gait events using wearable sensors, Neural Netw. 102 (2018) 107–119.
[9] M. Muaaz, R. Mayrhofer, Smartphone-based gait recognition: from authentication to imitation, IEEE Trans. Mobile Comput. 16 (11) (2017) 3209–3221.
[10] M. Nieto-Hidalgo, F.J. Ferrández-Pastor, R.J. Valdivieso-Sarabia, J. Mora-Pascual, J.M. García-Chamizo, Vision based gait analysis for frontal view gait sequences using RGB camera. International Conference on Ubiquitous Computing and Ambient Intelligence, Springer, Cham, 2016, pp. 26–37.
[11] C. MacDonald, et al., Determination of human gait phase using fuzzy inference, in: 2007 IEEE 10th International Conference on Rehabilitation Robotics, IEEE, 2007, pp. 661–665.
[12] T.M. Guess, S. Razu, A. Jahandar, M. Skubic, Z. Huo, Comparison of 3D joint angles measured with the kinect 2.0 skeletal tracker versus a marker-based motion capture system, J. Appl. Biomech. 33 (2) (2017) 176–181.
[13] J.A. Zeni Jr., J.G. Richards, J.S. Higginson, Two simple methods for determining gait events during treadmill and overground walking using kinematic data, Gait Posture 27 (4) (2008) 710–714.
[14] S.C. Wearing, S.R. Urry, J.E. Smeathers, The effect of visual targeting on ground reaction force and temporospatial parameters of gait, Clin. Biomech. 15 (8) (2000) 583–591.
[15] M. Roerdink, C.J.C. Lamoth, P.J. Beek, Online gait event detection using a large force platform embedded in a treadmill, J. Biomech. 41 (12) (2008) 2628–2632.
[16] Y. Qi, C.B. Soh, E. Gunawan, K.-S. Low, R. Thomas, Assessment of foot trajectory for human gait phase detection using wireless ultrasonic sensor network, IEEE Trans. Neural Syst. Rehabil. Eng. 24 (1) (2015) 88–97.
[17] Y. Wahab, N.A. Bakar, Gait analysis measurement for sport application based on ultrasonic system, in: 2011 IEEE 15th International Symposium on Consumer Electronics (ISCE), IEEE, 2011, pp. 20–24.
[18] J. Taborri, E. Palermo, S. Rossi, P. Cappa, Gait partitioning methods: a systematic review, Sensors 16 (1) (2016) 66.

[19] P. Chinmilli, S. Redkar, W. Zhang, T. Sugar, A review on wearable inertial tracking based human gait analysis and control strategies of lower-limb exoskeletons, Int. Robot. Autom. J. 3 (7) (2017) 00080.
[20] M.M. Skelly, H.J. Chizeck, Real-time gait event detection for paraplegic FES walking, IEEE Trans. Neural Syst. Rehabil. Eng. 9 (1) (2001) 59–68.
[21] S. Mohammed, A. Same, L. Oukhellou, K. Kong, W. Huo, Y. Amirat, Recognition of gait cycle phases using wearable sensors, Robot. Auton. Syst. 75 (2016) 50–59.
[22] X. Meng, H. Yu, M.P. Tham, Gait phase detection in able-bodied subjects and dementia patients, in: 2013 35th Annual International Conference of the IEEE Engineering in Medicine and Biology Society (EMBC), IEEE, 2013, pp. 4907–4910.
[23] T. Seel, J. Raisch, T. Schauer, IMU-based joint angle measurement for gait analysis, Sensors 14 (4) (2014) 6891–6909.
[24] D. Quintero, D.J. Lambert, D.J. Villarreal, R.D. Gregg, Real-time continuous gait phase and speed estimation from a single sensor, in: 2017 IEEE Conference on Control Technology and Applications (CCTA), IEEE, 2017, pp. 847–852.
[25] C. Fleischer, C. Reinicke, G. Hommel, Predicting the intended motion with EMG signals for an exoskeleton orthosis controller, in: 2005 IEEE/RSJ International Conference on Intelligent Robots and Systems, IEEE, 2005, pp. 2029–2034.
[26] J.L. Pons, Rehabilitation exoskeletal robotics, IEEE Eng. Med. Biol. Mag. 29 (3) (2010) 57–63.
[27] S. Lee, Y. Sankai, Power assist control for leg with hal-3 based on virtual torque and impedance adjustment, in: IEEE International Conference on Systems, Man and Cybernetics, vol. 4, IEEE, 2002, pp. 6-pp.
[28] F. Zhang, P. Li, Z.-G. Hou, Z. Lu, Y. Chen, Q. Li, M. Tan, sEMG-based continuous estimation of joint angles of human legs by using BP neural network, Neurocomputing 78 (1) (2012) 139–148.
[29] G.R. Naik, S. Easter Selvan, S.P. Arjunan, A. Acharyya, D.K. Kumar, A. Ramanujam, H.T. Nguyen, An ICA-EBM-based sEMG classifier for recognizing lower limb movements in individuals with and without knee pathology, IEEE Trans. Neural Syst. Rehabil. Eng. 26 (3) (2018) 675–686.
[30] C.D. Joshi, U. Lahiri, N.V. Thakor, Classification of gait phases from lower limb EMG: application to exoskeleton orthosis, in: 2013 IEEE Point-of-Care Healthcare Technologies (PHT), IEEE, 2013, pp. 228–231.
[31] G. Courtine, M. Schieppati, Human walking along a curved path. II. Gait features and EMG patterns, Eur. J. Neurosci. 18 (1) (2003) 191–205.
[32] R.T. Lauer, B.T. Smith, R.R. Betz, Application of a neuro-fuzzy network for gait event detection using electromyography in the child with cerebral palsy, IEEE Trans. Biomed. Eng. 52 (9) (2005) 1532–1540.
[33] S.W. Lee, T. Yi, J.-W. Jung, Z. Bien, Design of a gait phase recognition system that can cope with EMG electrode location variation, IEEE Trans. Autom. Sci. Eng. 14 (3) (2015) 1429–1439.
[34] J. Chen, X. Zhang, Y. Cheng, N. Xi, Surface EMG based continuous estimation of human lower limb joint angles by using deep belief networks, Biomed. Signal Process. Control 40 (2018) 335–342.
[35] A.L. Hof, H. Elzinga, W. Grimmius, J.P.K. Halbertsma, Speed dependence of averaged EMG profiles in walking, Gait Posture 16 (1) (2002) 78–86.
[36] X. Zhai, B. Jelfs, R.H.M. Chan, C. Tin, Self-recalibrating surface EMG pattern recognition for neuroprosthesis control based on convolutional neural network, Front. Neurosci. 11 (2017) 379.
[37] H.J. Hermens, B. Freriks, C. Disselhorst-Klug, G. Rau, Development of recommendations for SEMG sensors and sensor placement procedures, J. Electromyogr. Kinesiol. 10 (5) (2000) 361–374.
[38] A.G. Rainoldi, M.I. Caruso, A method for positioning electrodes during surface EMG recordings in lower limb muscles, J. Neurosci. Methods 134 (1) (2004) 37–43.
[39] M.H. Schwartz, A. Rozumalski, J.P. Trost, The effect of walking speed on the gait of typically developing children, J. Biomech. 41 (8) (2008) 1639–1650.
[40] G.R. Naik, S. Easter Selvan, S.P. Arjunan, A. Acharyya, D.K. Kumar, A. Ramanujam, H.T. Nguyen, An ICA-EBM-based sEMG classifier for recognizing lower limb movements in individuals with and without knee pathology, IEEE Trans. Neural Syst. Rehabil. Eng. 26 (3) (2018) 675–686.
[41] K. Cho, B. Van Merriënboer, C. Gulcehre, D. Bahdanau, F. Bougares, H. Schwenk, Y. Bengio, Learning Phrase Representations Using RNN Encoder-Decoder for Statistical Machine Translation, 2014 (arXiv preprint), arXiv:1406.1078.
[42] M. Atzori, M. Cognolato, H. Müller, Deep learning with convolutional neural networks applied to electromyography data: a resource for the classification of movements for prosthetic hands, Front. Neurorobot. 10 (2016) 9.
[43] M. Atzori, A. Gijsberts, C. Castellini, B. Caputo, A.-G. Mittaz Hager, S. Elsig, G. Giatsidis, F. Bassetto, H. Müller, Electromyography data for non-invasive naturally-controlled robotic hand prostheses, Sci. Data 1 (1) (2014) 1–13.
[44] M. Sokolova, G. Lapalme, A systematic analysis of performance measures for classification tasks, Inf. Process. Manage. 45 (4) (2009) 427–437.
[45] Y. Hu, Y. Wong, W. Wei, Y. Du, M. Kankanhalli, W. Geng, A novel attention-based hybrid CNN-RNN architecture for sEMG-based gesture recognition, PLOS ONE 13 (10) (2018) e0206049.
[46] G.S. Murley, H.B. Menz, K.B. Landorf, A.R. Bird, Reliability of lower limb electromyography during overground walking: a comparison of maximal-and sub-maximal normalisation techniques, J. Biomech. 43 (4) (2010) 749–756.
[47] M.O. Ericson, R. Nisell, J. Ekholm, Quantified electromyography of lower-limb muscles during level walking, Scand. J. Rehabil. Med. 18 (4) (1986) 159–163.
[48] J.-H. Ryu, D.-H. Kim, Multiple gait phase recognition using boosted classifiers based on sEMG signal and classification matrix, Proceedings of the 8th International Conference on Ubiquitous Information Management and Communication (2014) 1–4.